Global imaging of O^+ from IMAGE/HENA

Donald G. Mitchell, Pontus C:son Brandt and Edmond C. Roelof
The Johns Hopkins University Applied Physics Laboratory, Laurel, MD, USA

Douglas C. Hamilton, Kyle C. Retterer
The University of Maryland, College Park, MD, USA

Steven Mende
Space Science Laboratory, Berkeley, CA, USA

Abstract. The magnetospheric O^+ population in the 52-180 keV range during storms is investigated through the analysis of energetic neutral atom (ENA) images. The images are obtained from the high energy neutral atom (HENA) imager onboard the IMAGE satellite. At each substorm onset following the commencement of a geomagnetic storm the oxygen ENA display ∼30 min intense bursts. Only very weak corresponding features in the 60-119 keV hydrogen ENA can be occasionally seen. The dominating fraction of the oxygen ENA emissions are produced when O^+ ions mirror/precipitate at low altitudes, where the number density of the neutral atmosphere is high. During the storm we observed several bursts of oxygen ENA, but it is still not clear how much the O^+ content of the ring current increases during the storm main phase. Our observations suggest that the responsible injection mechanism is mass-dependent and scatters the pitch angles. This leads us to favor a non-adiabatic mechanism proposed by (Delcourt, 2002).

Keywords: ENA imaging, substorm, oxygen, dipolarization, precipitation

1. Introduction

The presence of oxygen in the ring current has been known for many years (Hamilton et al., 1988). Furthermore, this oxygen has been shown to be of ionospheric origin, as it is singly charged. Since the generation of ENA requires energetic singly charged ions to charge exchange with cold neutral gas atoms (in the case of Earth, the hydrogen geocorona), the ring current should emit oxygen atoms when O^+ is present, along with the hydrogen it normally emits when energetic protons are present. (Hamilton et al., 1988) and many others have shown that oxygen has a relatively brief residence time in the ring current. The reasons for this are (1) a large charge exchange cross section for O^+ on H (relative to the smaller proton on H cross section) (Phaneuf et al., 1987), and (2) a larger gyroradius, making the oxygen more susceptible to pitch-angle scattering by current-sheet scattering and subsequent loss to the atmosphere. Although it has been known for some time that the oxygen content of the ring current depends on the magnitude of a geomagnetic storm (as measured by the storm index, *Dst*), it has not been possible

to observe the oxygen injection process globally, and so the precise timing and circumstances under which it was injected have been the subject of some speculation. The same can be said for the loss of oxygen from the ring current. Its loss was measured from one orbit to the next of spacecraft that cut through the storm-time ring current, but no continuous monitor of the oxygen content, nor the process by which the oxygen was lost from the system, has been available before now. With the IMAGE mission, using the HENA imager, we have now at least partial answers to some of these questions.

2. Observations

2.1. OXYGEN SEPARATION WITH HENA

Since its in-flight commissioning in May 2000, the HENA instrument on the IMAGE spacecraft (Burch, 2000) has imaged the Earth's ring current nearly continuously. Although the HENA instrument (Mitchell et al., 2000) included a subsystem that was to have provided species identification, that subsystem never functioned properly. Analysis of data from the main, microchannel plate (MCP) based subsystem showed that oxygen and hydrogen could be separately identified using time of flight (TOF) measurement combined with MCP pulse-height. The flight software was modified in August of 2001, and since then HENA has produced ENA images in both hydrogen and oxygen. To illustrate the instrument response to species, we include Figures 1 and 2, which shows two scatter plots of energy/nucleon versus stop MCP pulse-height. The data in Figure 1 was obtained before the storm of 12 August 2000 as indicated in the *Dst* inset in the upper left corner of the plot. Figure 2 shows the data from the storm main phase as indicated in the *Dst* plot. Here we can see that two populations stand out distinctly. The lower population is oxygen. If helium were present in significant quantity, the region between these two groups would be filled with points, and separation by this technique would not be very productive. The reason for the lack of Helium atoms is probably due to the charge exchange cross section of He^+ ions on geocoronal hydrogen (Phaneuf et al., 1987). The cross section peaks at $2{\cdot}10^{-16}$ cm^{-2} around 10 keV/nucleon and drops dramatically on both sides. The charge exchange cross section for protons on hydrogen for this energy (per nucleon) is about four times higher. The cross section for O^+ on hydrogen at 10 keV/nucleon is about the same as that of He^+ and increases at lower energies (Phaneuf et al., 1987). In order to clarify this argument let us assume that the He^+ flux for this storm was equal to that of the protons; the

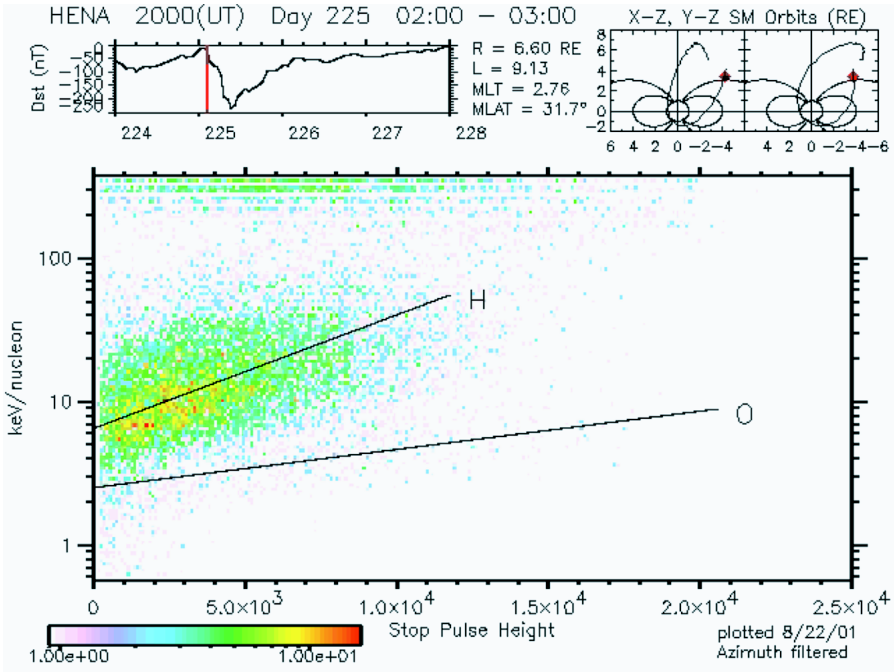

Figure 1. A plot showing the energy per nucleon versus the stop MCP pulse height. In such a plot the counts from each species lies on a straight line. This fact allowed the oxygen ENA to be separated from the hydrogen ENA in the HENA imager. This data was obtained before the 12 August 2000 storm as can be seen in the *Dst* inset in the upper left corner.

resulting helium ENA count rate would be four times less than that of the hydrogen ENAs at 10 keV/nucleon. Using Figure 2 this would result in a helium ENA count rate down in the purple-blue end of the colorbar, which is consistent with the count rate between the hydrogen and oxygen line in Figure 2. Now, in reality the He^+ flux is smaller than the proton flux, which makes this an upper limit estimate. Through all storms analyzed using this technique, helium has never been present in noticeable numbers in this format. Using this understanding of the HENA instrument response to species, the flight software was revised to separate hydrogen from oxygen on an event-by-event basis, and bin to images separately in each species.

Although we have added the capability for separately imaging oxygen, the angular resolution of the oxygen images is only marginal. The HENA sensor relies on a relatively thick entrance foil to filter out the majority of the ultraviolet light that can trigger its MCP sensors. This foil scatters ENA in the entrance slit, and degrades the resolution that can be realized (see [Mitchell et al., 2000] for a more

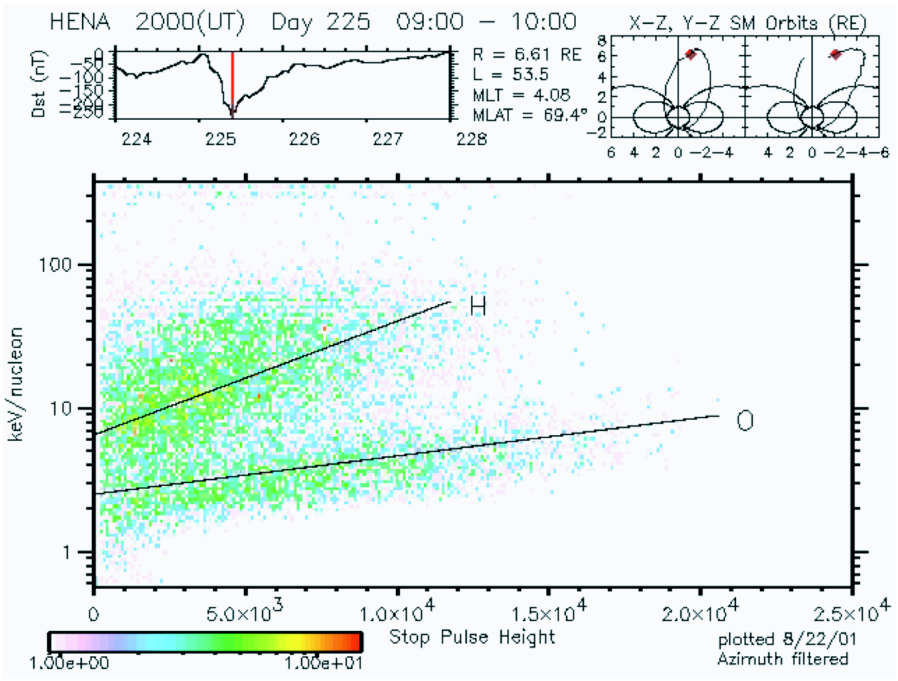

Figure 2. Same format as Figure 1, but this data was obtained in the mainphase of the storm as can be seen in the *Dst* inset in the upper left corner. Note the increase of the second (lower population) which is oxygen ENAs.

complete discussion). Therefore, when the spacecraft is near apogee, any bright emission source in oxygen tends to spread sufficiently that it masks any adjacent weaker sources that might be present. Since typically the brightest ENA emission of any species is generated when low altitude, mirroring ions interact with the dense neutral atmosphere in the oxygen exobase, strong low altitude emission often overwhelms the weaker emission from the high altitude ring current. Nevertheless, the HENA oxygen measurements since August 2001 reveal an intriguing relationship between storm-time O^+ enhancements in the ring current, and substorm activity.

2.2. THE SUBSTORM CONNECTION

Figure 3 shows ENA images during a substorm on 21 October 2001, in hydrogen (top) and oxygen (bottom), each image accumulated over 10 min. The top row (Figure 3a-3c) shows the 27-60 keV hydrogen, and the bottom row (Figure 3d-3f) shows the 52-180 keV oxygen. For this particular event the substorm onset occured at around 23:23 UT. Note that for the purpose of comparison we have individual colorbars

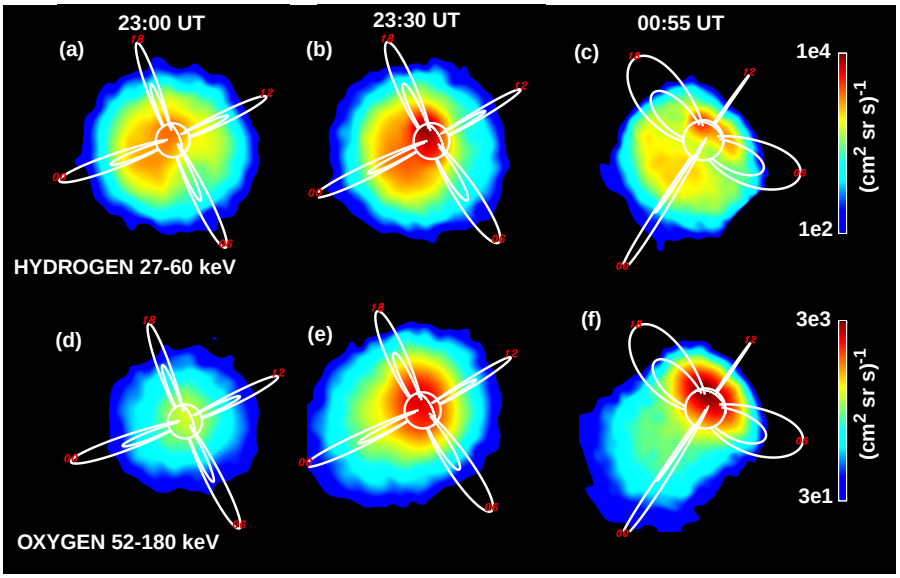

Figure 3. A sequence of ENA images obtained during a substorm injection during the 21-22 October 2001 storm. The top row (a)-(c) shows the hydrogen in the 27-60 keV range and the bottom row (d)-(f) shows the oxygen in the 52-180 keV range. Note domination of oxygen from low altitudes at 00:55 UT as compared to the one for hydrogen. Note also that the colorbars have been scaled individually for each row.

for hydrogen and oxygen, but with the same range within each species (row). We can see that there is indeed an increase of the hydrogen ENA emissions both from the Earth as well as off the limb. For oxygen it appears that the emissions are centered on the Earth, with much less increase off the limb. This tells us that the ratio between the ENAs produced by precipitating/mirroring ions and those produced by the near-Earth ring current ions, is much higher for oxygen than that of hydrogen. It is the ENAs produced by the O^+ population mirroring at low altitudes that dominate the bursts in the ENA data. However, there are clear indications that the high altitude oxygen emissions increases in the bursts, too.

In Figures 4 and 5, the HENA image data is displayed in a more compact form for the same period. Over the course of a spacecraft spin, the HENA sensor images the entire sky from 60° above to 60° below the spacecraft spin plane. We refer to the angle swept by this motion as the image azimuth, and the angle relative to the spin plane as elevation. The plots are created by averaging the data in the images over the elevation angle, while retaining full resolution in azimuth. Each spin (two minutes of data) becomes one vertical line in a plot. The three plots cover the

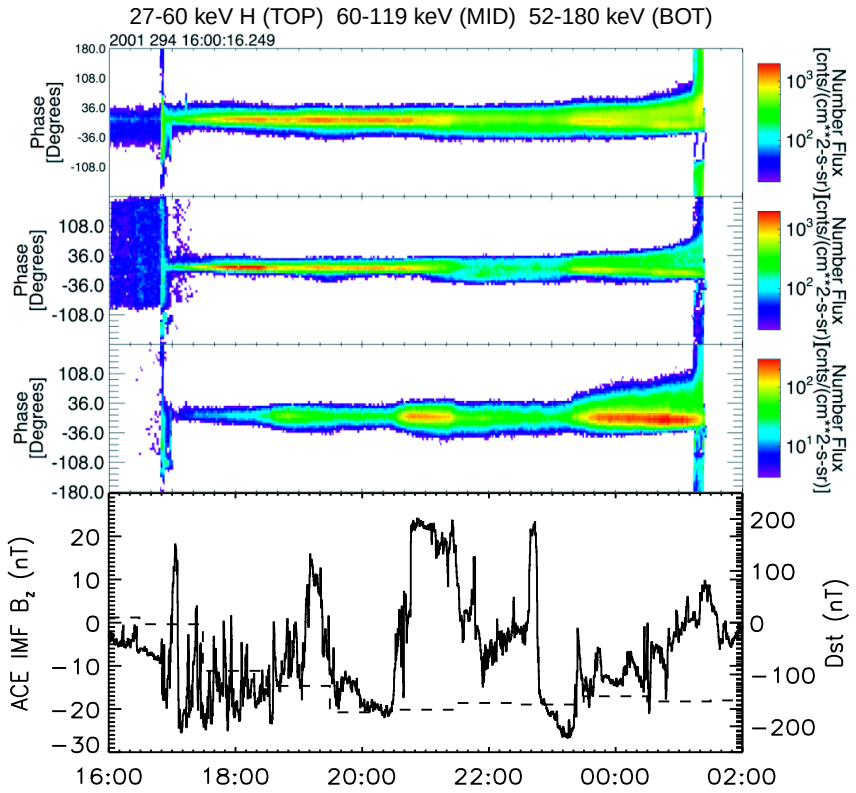

Figure 4. A spin angle-time diagram of the ENA data for the entire day of 21 October 2001. Spin angle of the instrument is on the vertical axis and time is on the horizontal. The elevational dimension fo the instrumental image has been summed in to a one-pixel wide column. The top panel is hydrogen ENA in the 27-60 keV range, the middle panel is the hydrogen ENA in the 60-119 keV range, and the bottom panel shows the oxygen ENA data in the 52-180 keV range. The lowest panel shows the IMF B_z (solid line) obtained by the ACE spacecraft (lagged for the arrival at the center of Earth) and the *Dst* index (dashed line).

hydrogen energy range of 27 to 60 keV (top), the hydrogen energy range of 60 to 120 keV (middle), and the oxygen energy range of 52 to 180 keV (bottom). The IMF B_z (solid line) from the ACE spacecraft is plotted together with the *Dst* index (dashed line) in the bottom panel of each figure.

Figure 4 is obtained during the geomagnetic storm of 21 October 2001 where the storm commenced at about 17:00 UT as the IMF B_z dropped below zero. The elevated background prior to onset is caused by an energetic storm particle (ESP) event associated with the passage of a shock in the solar wind. The high ion flux in the interplanetary medium at this time has direct access to IMAGE (situated in the cusp)

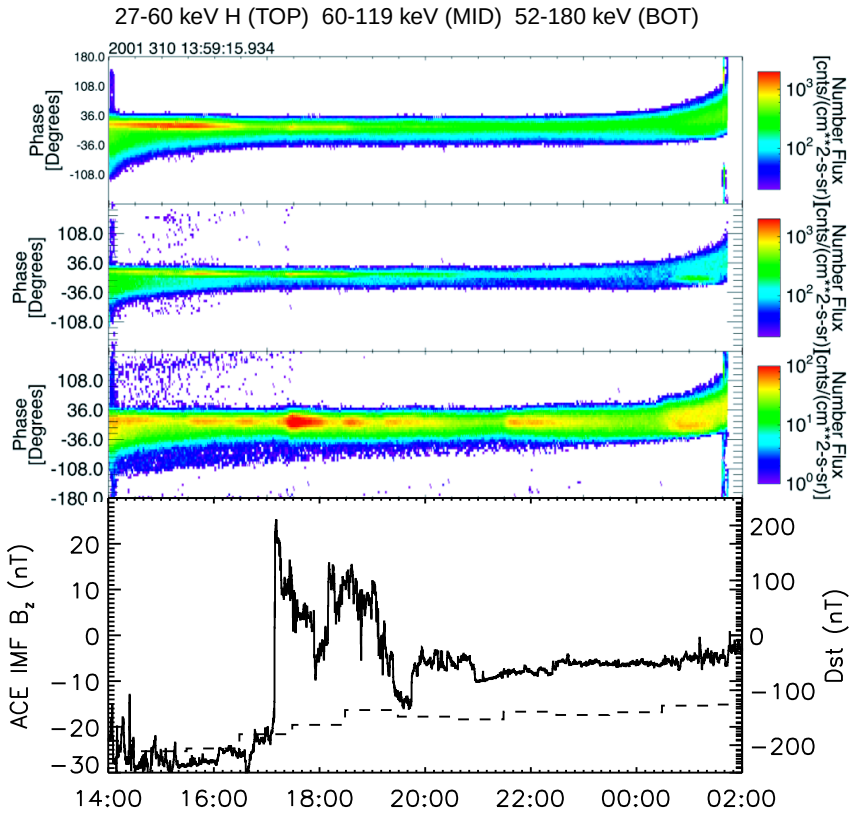

Figure 5. The same format as Figure 4, but for the 6 Novemeber 2001 storm.

along open field lines, and the HENA charged particle rejection plates only reject about four orders of magnitude of the incident ion flux. Still, the sharp increase in ENA emission can be seen clearly in all species.

Figure 5 shows the ENA data for a more complicated storm on 6 November 2001. Here the IMF B_z was around -30 nT for a long time and then started fluctuating around zero during the evening of the same day, causing multiple substorms. For the same day we see repetitive bursts in the oxygen data during the evening. Later that day the fluctuations in IMF B_Z settled down around -5 nT, but still with some moderate substorm activity.

Characteristic of most storms observed by HENA since we began separating oxygen, is that the oxygen ENA emission is not at its peak near the beginning of the storm (as is common for hydrogen), but rather grows by sudden enhancements several hours into the storm. How much the O^+ content of the ring current increases during the storm is the subject of a future paper and will not be covered here. We will show below that every sudden burst in oxygen ENA intensity seen in the

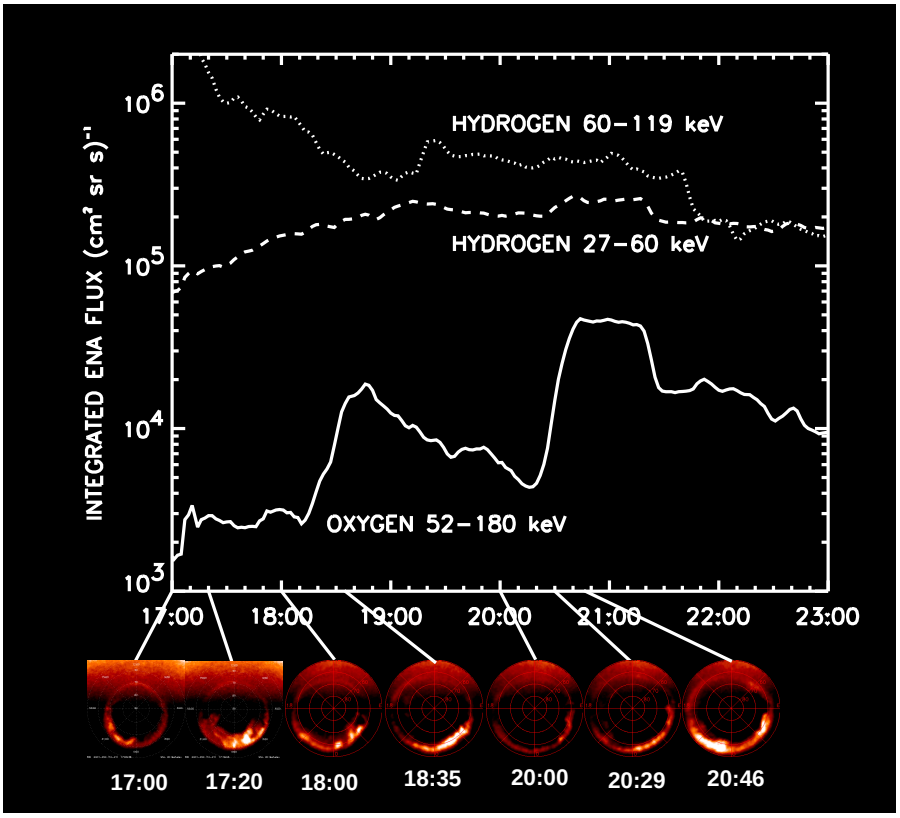

Figure 6. Plot showing the ENA intensity during the 21 October 2001 storm. The intensity was obtained by integrating over a 30°×30° box in the ENA images centered at the Earth for oxygen and hydrogen at energies as indicated. The images below the line plot are the auroral FUV images obtained by the WIC onboard IMAGE mapped to geomagnetic surface coordinates. Lowest latitude is 50° and noon is up. Note how the correlation between the oxygen ENA bursts and the auroral substorm onsets.

bottom panel of Figures 4 and 5 is well correlated with a substorm onset.

Figure 6 shows the ENA intensities integrated over a 30°×30° box centered on earth for hydrogen and oxygen and different energies as indicated. The data is obtained during the 21 October 2001 storm. The square images below the plot are the auroral images obtained by the far ultra violet (FUV) wideband imaging camera (WIC) in the 140-160 nm range onboard the IMAGE spacecraft and show the electron aurora mapped to geomagnetic surface coordinates. The lowest latitude is 50° in the auroral image and noon is up. The dayside is directed up in the plot. We only have auroral data until 21:00 UT, but we can see a clear correlation between the auroral substorm onset and the

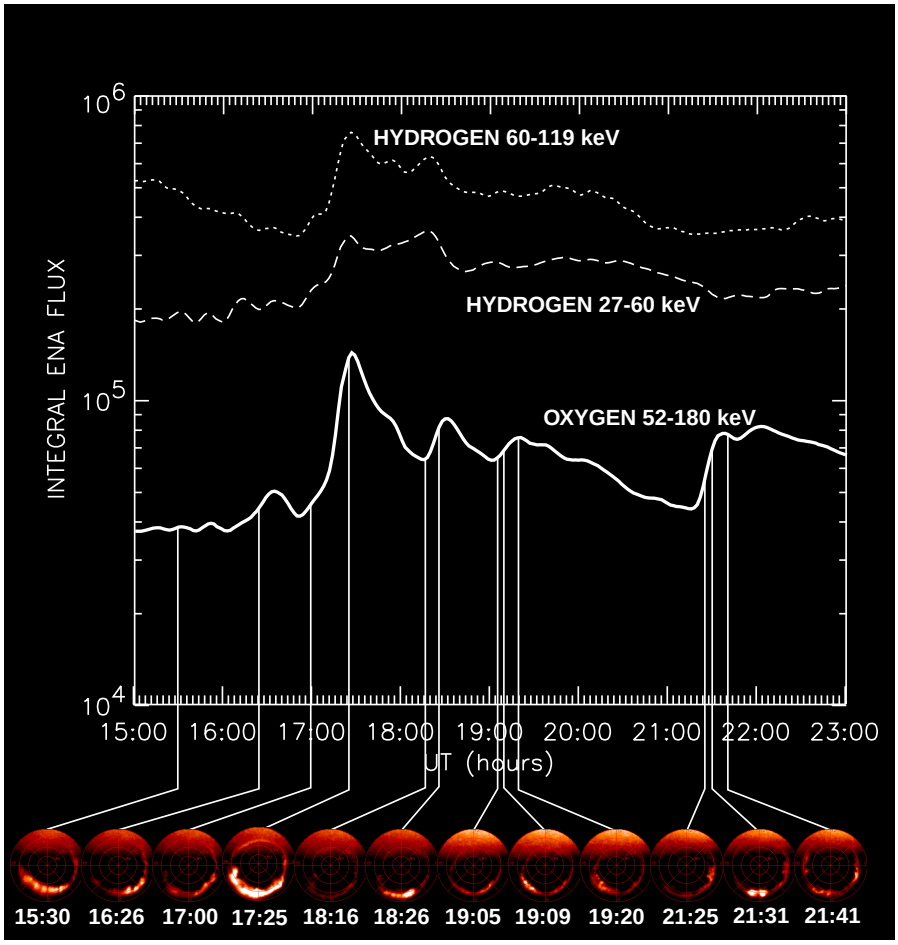

Figure 7. Same as Figure 6 but for the 6 November 2001 storm. Note the weaker signatures in the hydrogen ENA intensity at 17:25, 18:22, and 19:20 UT.

oxygen ENA bursts. The plots of hydrogen in Figure 6 show no clear peaks at the time of each substorm onset. The first substorm of 21 October occured at about 17:20 UT. The storm commenced around 17:00 UT when the IMF B_z decreased suddenly down to -25 nT. Note how relatively weak the oxygen ENA burst is at 17:20 compared to the two later in the storm main phase at 18:35 and 20:46 UT. This supports the idea that the oxygen ENA bursts are caused by the energization of preexisting O^+ in the plasmasheet. Early in the storm, ionospheric O^+ ions have not had time to be convected to the plasmasheet. However, when the IMF B_z has been negative for a couple of hours, ionospheric outflow has enhanced the O^+ densities in the plasmasheet (Cladis, 1986), so that there is a significant amount to energize.

Figure 7 shows the ENA intensities in the same format as for Figure 6, but for the 6 November 2001 storm. We can see several peaks in the oxygen ENA at around 16:30, 17:30, 18:30, 19:20, and 21:35 UT. We see that the substorm expansion onset starts just as the oxygen ENA flux starts increasing. Only the 17:25 substorm has clear simultaneous signatures in both the high and low energy hydrogen as well as the oxygen. For all other substorms the hydrogen have only a weak or no similar feature. It is interesting to note that the peak in oxygen ENA intensity at 18:30 UT is preceded by smaller peaks in the hydrogen ENA intensities at 18:22 UT. The same behavior can be seen for the peak in oxygen at 19:20 UT. We do not have an explanation for this occasional time difference.

Bursts of oxygen ENAs are commonly seen during the storms when IMF B_z has been negative for long periods. During isolated substorms (IMF B_z more positive), we have not yet seen bursts of oxygen. This immediately suggests that oxygen bursts are related to the magnitude of the stretching of the magnetic field relatively close to the Earth (which only occurs during large storms) and from Figures 6 and 7 it appears that the magnitude of the burst is related to the magnitude of the auroral substorm as manifested in the FUV intensities. More events and studies are needed before any quantitive conlcusion can be drawn.

3. Discussion

We have seen that the 52-180 keV oxygen ENA intensity increases in bursts for each substorm onset during storm periods. The hydrogen behaves differently, although there are occasional similar, but weaker signatures for the 60-119 keV hydrogen. The fact that the oxygen behaves differently from the hydrogen in storms is perhaps not surprising, even though we did not expect it. The energy ranges are somewhat different, the sources may be at least in part different, and the dominant loss mechanisms are probably different. At energies greater than 100 keV, the oxygen will gradient and curvature drift much faster than the lower energy hydrogen, which may contribute to a faster loss from the magnetosphere if the drift trajectories are open. Furthermore, the oxygen ions have about four times larger gyroradii than the protons at the same energy, causing them to be much more subject to pitch angle scattering and other gyroradius-dependent effects than the hydrogen.

The ENA images appear to support the notion that substorms are an important component in the mechanism that supplies oxygen from the ionosphere to the storm time ring current, and that they may also be an important component in the oxygen loss mechanisms. The large

oxygen enhancements seen in the ENA images near substorm onset are almost certainly dominated by low altitude ENA emission. This sudden strong low altitude emission is what is expected if a trapped distribution suddenly is pitch angle scattered, filling the loss cone. Under those circumstances, the ions would begin mirroring at lower altitudes, where they would interact with the oxygen exobase. This would produce strong ENA emission, both because the neutral gas density is an exponential function of altitude, and because the charge exchange cross section for oxygen ions on oxygen (Torr et al., 1974) is considerably higher than that for oxygen ions on hydrogen (Phaneuf et al., 1987), the dominant species in the exosphere. Oxygen outflow during periods of enhanced substorm electric fields, as well as during enhanced convection, have been known for a long time (Yau and André, 1997), so the mechanism to supply oxygen to the ring current is at least in part supplied by substorms.

However, the oxygen must then be accelerated from a few eV up to over a hundred keV, and be transported from the low altitude, high latitude magnetosphere to the 3-5 R_E equatorial ring current at the same time. As the oxygen flows out from the ionosphere along the field, it will be $\mathbf{E}\times\mathbf{B}$ drifted into the near-Earth plasmasheet, where it can be convected in to ring current altitudes (Cladis, 1986). In this process, the oxygen will gain energy both from centrifugal acceleration and from the adiabatic energization. However, this process is not sufficient to produce >100 keV O^+ on ∼10 min timescales (Cladis and Francis, 1992).

(Delcourt, 2002) simulated the acceleration mechanism for different species during a typical substorm dipolarization. The dipolarization was reproduced by stepping a Tsyganenko-89 (Tsyganenko, 1989) magnetic field configuration from Kp=5 to Kp=2 during 1 min. (Delcourt, 2002) launched O^+ ions from the high-latitude ionosphere with an initial energy of 100 eV and then let them be transported in the time-dependent field. Without a dipolarization (static magnetic field) the O^+ ions reached 10s of keV. With dipolarization the O^+ ions reached an energy of 100s of keV. Furthermore, (Delcourt, 2002) found that the pitch angle distributions changed rapidly to more field aligned distributions, and therefore contributed to a significant precipitation. This process is an effect of the non-adiabatic heating that occurs for any ions whose gyrofrequency is comparable to the timescales of the dipolarization. Since protons have a gyro period which is 16 times shorter than that of O^+, this process would mainly effect the O^+. Other relevant studies have also been done by (Delcourt et al., 1990; Delcourt et al., 1991; Delcourt and Moore, 1992).

As can be seen from Figure 4 the initial oxygen response at the beginning of the storm is relatively weak, probably because there is

little oxygen in the plasma sheet before the storm. After that time, the ionospheric oxygen has had time to escape from the ionosphere; the atmosphere will have been heated by Joule heating and precipitation, and the O^+ will have been ionized by energetic electron impact; strong parallel electric fields will have developed to extract the oxygen from its altitude range in the ionosphere, and storm and substorm-associated waves will also accelerate the oxygen in conics. After several hours of continued convection (IMF B_z <0) the ring current will have an enhanced O^+ content. Whether this is due to enhanced convection or due to the substorm O^+ injection becoming trapped is still under investigation.

Because the angular resolution of HENA is poor in the oxygen emission, it is difficult to separately monitor the high altitude, equatorial ring current emission as well as the low altitude emission. Therefore, it is difficult to see from the ENA images whether the sudden brightening observed is entirely due to enhanced precipitation, or if there is a fresh injection of oxygen into the ring current also associated. What is clear, from Figure 3, is that the ratio of the high altitude emission to the low altitude emission is very different for oxygen than it is for hydrogen. Both the hydrogen and oxygen images in the right-most column of Figure 3 show enhanced emission from the footpoints of the magnetic field in the northern hemisphere, but the hydrogen emission from low altitude is only about a factor of two brighter than the high altitude emission from the tail (foreground), whereas for the oxygen, the low altitude emission is more than an order of magnitude higher than the high altitude emission. This is direct evidence that the oxygen is being lost from the system at a much higher rate, relative to its high altitude flux, than is the hydrogen. This suggests that while flow-out losses may also be important, precipitation losses cannot be ignored for the oxygen. Furthermore, to the extent that precipitation losses are important, substorm dynamics are also important to the oxygen content of the storm time ring current (both in terms of supply, and loss).

4. Summary and Conclusions

We have analyzed global oxygen ENA data in the 52-180 keV range from the HENA imager onboard the IMAGE satellite. During geomagnetic storms when the magnetospheric convection is enhanced, ∼30 min bursts of oxygen ENA appear in the images centered on the Earth. Due to the scattering in the front foil of the instrument for the particle velocities at these energies, the angular resolution makes it difficult at this stage to say how much of the burst come from O^+

in the inner magnetosphere versus how much that comes from the O^+ precipitating/mirroring at low altitudes. The ratio between the low- and high-altitude ENA emissions for hydrogen is less than that of oxygen. The start of the increase in the oxygen ENA intensity is well correlated with the auroral substorm onset and therefore also probably well correlated with the substorm dipolarization. The bursts seen in the oxygen ENA data do not appear clearly in the hydrogen ENA data (27-119 keV). Simulations (André et al., 1998; Cladis and Francis, 1992) and observations (Yau and André, 1997) of O^+ outflow processes show that they are probably insufficient to energize the ionospheric O^+ up to several 100s keV.

(Delcourt, 2002) showed that a one minute dipolarization would energize the O^+ ions up to several 100s of keV, whereas protons only would gain 10s of keV for the same process, consistent with our observations. The reason for this is that the gyro period of an O^+ ion is comparable to the timescale of the electric field induced by the dipolarization.

Acknowledgements

We thank D. Dominique for fruitful discussions regarding the possible energization mechanism of the O^+. Also thanks to the IMAGE FUV-team at The Space Science Laboratory in Berkeley, CA, for providing auroral FUV data.

References

André, M., P. Norqvist, L. Andersson, L. Eliasson, A. I. Eriksson, L. Blomberg, R. E. Erlandsson, and J. Waldemark: 1998, 'Ion energization mechanism at 1700 kilometer in the auroral region'. *J. Geophys. Res.* **103**, 4199–4222.

Burch, J. L. (ed.): 2000, *The IMAGE mission*. Kluwer Academic. Reprinted from *Space Sci. Rev.*, vol. 91, Nos. 1-2, 2000.

Cladis, J. B.: 1986, 'Parallel acceleration and transport of ions from polar ionosphere to plasma sheet'. *Geophys. Res. Lett.* **13**(9), 893–896.

Cladis, J. B. and W. E. Francis: 1992, 'Distribution in the magnetotail of O^+ ions from cusp/cleft ionosphere: a possible substorm trigger'. *J. Geophys. Res.* **97**(A1), 123–130.

Delcourt, D. C.: 2002, 'Particle acceleration by inductive electric fields in the inner magnetosphere'. *J. of Atmosph. and Solar-Terr. Phys.* **64**, 551–559.

Delcourt, D. C. and T. E. Moore: 1992, 'Precipitation of ions induced by magnetotail collapse'. *J. Geophys. Res.* **97**(A5), 6405.

Delcourt, D. C., T. E. Moore, and J. A. Sauvaud: 1991, 'Gyro-phase effects near the storm time boundary of energetic plasma'. *Geophys. Res. Lett.* **18**(8), 1485.

Delcourt, D. C., J. A. Sauvaud, and T. E. Moore: 1990, 'Cleft O^+ contribution to the ring current'. *J. Geophys. Res.* **95**, 20937.

Hamilton, D. C., G. Gloeckler, F. M. Ipavich, W. Studemann, B. WIlken, and G. Kremser: 1988, 'Ring current development during the great geomagnetic storm of February 1986'. *J. Geophys. Res.* **93**(A12), 14343–14355.

Mitchell, D. G., S. E. Jaskulek, C. E. Schlemm, E. P. Keath, R. E. Thompson, B. E. Tossman, J. D. Boldt, J. R. H. abd G. B. Andrews, N. Paschalidis, D. C. Hamilton, R. A. Lundgren, E. O. Tums, P. Wilson IV, H. D. Voss, D. Prentice, K. C. Hsieh, C. C. Curtis, and F. R. Powell: 2000, 'High energy neutral atom (HENA) imager for the IMAGE mission'. *Space Sci. Rev.* **91**, 67–112.

Phaneuf, R. A., R. K. Janev, and M. S. Pindzola: 1987, 'Atomic Data for Fusion. Volume 5: Collisions of Carbon and Oxygen Ions with Electrons, H, H_2, and He'. Technical Report ORNL-6090, Oak Ridge National Lab., TN, USA.

Torr, M. G., J. C. G. Walker, and D. G. Torr: 1974, 'Escape of Fast Oxygen from the Atmosphere during Geomagnetic Storms'. *J. Geophys. Res.* **79**(34), 5267–5274.

Tsyganenko, N. A.: 1989, 'A magnetospheric magnetic field model with a warped tail current sheet'. *Planetary and Space Sci.* **37**, 5–20.

Yau, A. W. and M. André: 1997, 'Source of ion outflow in the high latitude ionosphere'. *Space Sci. Rev.* **80**, 1–25.